Supporting Information

A triple hydrogen-bond dominated fluorescent probe for monitoring the melting transition of polyurethane

Yuanyuan Guo,[a‡] Geng Li,[a‡] Hongyu Jiang,[a] Yaxing Tang,[a] Hua Wang,[a,b] Jie Li*[a] and Kunpeng Guo*[a]

[a]*Ministry of Education Key Laboratory of Interface Science and Engineering in Advanced Materials, Taiyuan University of Technology, Taiyuan 030024, China*

[b]*College of Textile Engineering, Taiyuan University of Technology, Jin Zhong, 030600, China*

E-mail: lijie01@tyut.edu.cn

guokunpeng@tyut.edu.cn

Table of contents

I. Experimental

General Methods

All chemicals and solvents were used as received from Energy Chemical Ltd. without further purification. NMR spectra measurements were carried out using a Bruker 400 spectrometer at 400 MHz for ^{1}H NMR and 101 MHz for ^{13}C NMR using chloroform-*d* as the solvent. All chemical shifts are reported in the standard d notation of parts per million. Flourier-transform infrared (FT-IR) spectra was characterized on a Bruker Tensor 27 spectrometer in the range of 3500−1000 cm^{-1}, using KBr pellets. (Temperature-dependent) photoluminescence (PL) spectra were taken on an Edinburgh Instrument FLS980 spectrometer equipped with a xenon lamp and Oxford OptistatDN cryostat. Gel permeation chromatography (GPC) was recorded by Aglient PL-GPC50 with THF as the mobile phase and narrow linear PMMA as the standards (550Da-955 kDa) . Differential scanning calorimeter (DSC) curve was obtained on a Mettler DSC3 under N_2 at heating of 20 K/min.

Synthesis and characterization

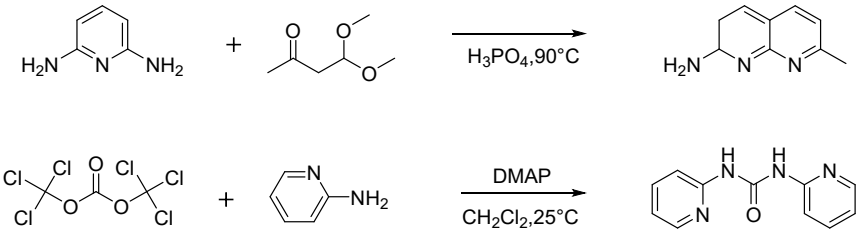

Scheme S1. Synthetic routes to **D-Ny** and **A-Py**.

Synthesis of 7-methyl-1,8-naphthyridin-2-amine (D-Ny)

2,6-Diaminopyridine (2.98 g, 27.31 mmol) and phosphoric acid (35.00 g) were by heating at 90 °C with stirring. Then 4,4-dimethoxy-2-butanone (3.73 mL, 28.11 mmol) was added drop-wise over a period of 30 min. The reaction mixture was stirred at 115 °C for 3 h. Upon cooling to room temperature, ammonium hydroxide was added dropwise to increase the pH value up to 10. The mixture was extracted with dichloromethane (3 × 100 mL). The resulting organic phase was washed with saturated aq. NaCl (2 × 100 mL), dried over $MgSO_4$, filtered and concentrated under reduced pressure. The crude product was recrystallized from tetrahydrofuran and petroleum ether to obtain **D-Ny** as yellow powders (3.31 g, 20.8 mmol, 76% yield). ^{1}H NMR (400 MHz, $CDCl_3$) δ 7.81-7.84 (m, 2H), 7.08 (d, J =8.0 Hz, 1H), 6.72 (d, J =12.0 Hz, 1H), 5.06 (s, 2H), 2.69 (s, 3H) . ^{13}C NMR (101 MHz, $CDCl_3$) δ 162.01, 159.55, 156.25, 137.94, 136.18, 118.79, 115.28, 111.50, 25.41.

Synthesis of 1,3-di(pyridin-2-yl)urea (A-Py)

Compounds 2-aminopyridine (1.50 g, 15.94 mmol) and 4-(dimethylamino)pyridine (DMAP) (2.32 g, 19.00 mmol) were dissolved in dichloromethane (15 mL). Bis(trichloromethyl)carbonate (0.95 g, 3.20 mmol) was dissolved in dichloromethane (10 mL) and the solution was added dropwise over a period of 1 h. The resulting mixture was stirred at room temperature and monitored by thin layer chromatography. The unreacted bis(trichloromethyl)carbonate was removed by bubbled with nitrogen and the solvent was evaporated under reduced pressure. The crude product was purified by column

chromatography (eluent: petroleum ether/ethyl acetate =1/1, v/v) to give **A-Py** as white crystals (1.30 g, 6.06 mmol, 76% yield). ^{1}H NMR (400 MHz, $CDCl_3$) δ 8.36-8.38 (m, 2H), 7.67-7.72 (m, 2H), 6.99 (t, J =12.0 Hz, 2H). ^{13}C NMR (101 MHz, $CDCl_3$) δ 153.68, 152.54, 147.28, 138.35, 118.22, 113.21.

Synthesis of polyurethanes

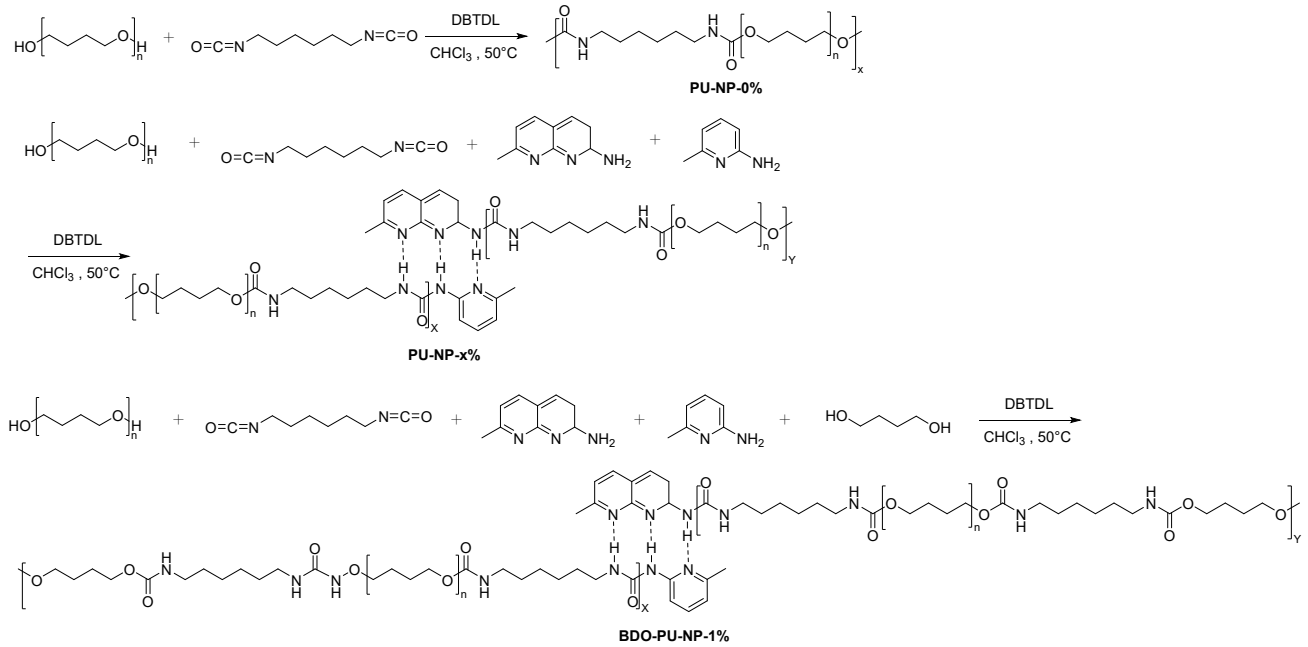

Scheme S2. Synthetic routes to the PUs.

PU-NP-0%: Dibutyltin dilaurate (DBTDL) (2 drops) was added to a stirred mixture of hydroxyl-terminated poly(tetrahydrofuran) (M_n=1,000 g/mol, 5.00 g, 5.00 mmol) and 1,6-diisocyanate (0.80 mL, 4.95 mmol) in $CHCl_3$ (20 mL), and the mixture was stirred at r.t. for 2 h. Then the reaction mixture was stirred at 50 °C for 48 h to produce a viscous solution. Then, the reaction mixture was cooled to room temperature and poured into hexane (1000 mL). The precipitate was filtered off and dried in vacuo to afford **PU-NP-0%** as a rubbery solid.

PU-NP-1%: Dibutyltin dilaurate (DBTDL) (2 drops) was added to a stirred mixture of hydroxyl-terminated poly(tetrahydrofuran) (M_n=1,000 g/mol, 5.00 g, 5.00 mmol) and 1,6-diisocyanate (0.80 mL, 4.95 mmol) in $CHCl_3$ (20 mL), and the mixture was stirred at r.t. for 2 h. A solution of **D-Ny** (8.0 mg,

0.05 mmol) and 2-amino-6-methylpyridine (5.4 mg, 0.05 mmol) in $CHCl_3$ (10 mL) was then added and the reaction mixture was stirred at 50 °C for 48 h to produce a viscous solution. Then, the reaction mixture was cooled to room temperature and poured into hexane (1000 mL). The precipitate was filtered off and dried in vacuo to afford **PU-NP-1%** as a rubbery solid (9.10 g, 88%, M_n = 99.626 kDA).

PU-NP-0.5%: Following the procedure of **PU-NP-1%**, a solution of **D-Ny** (4.00 mg, 0.025 mmol) and 2-amino-6-methylpyridine (2.70 mg, 0.025 mmol) in $CHCl_3$ (10 mL) was added.

PU-NP-2%: Following the procedure of **PU-NP-1%**, a solution of **D-Ny** (16 mg, 0.10 mmol) and 2-amino-6-methylpyridine (10.8 mg, 0.10 mmol) in $CHCl_3$ (10 mL) was added.

BDO-PU-NP-1%: Dibutyltin dilaurate (DBTDL) (2 drops) was added to a stirred mixture of hydroxyl-terminated poly(tetrahydrofuran) (M_n=1,000 g/mol, 2.50 g, 2.50 mmol) and 1,6-diisocyanate (0.80 mL, 4.95 mmol) in $CHCl_3$ (20 mL), and the mixture was stirred at r.t. for 2 h. A solution of **D-Ny** (8.00 mg, 0.05 mmol), 2-amino-6-methylpyridine (5.40 mg, 0.05 mmol) and butane-1,4-diol (0.23 g, 2.50 mol) in $CHCl_3$ (10 mL) was then added and the reaction mixture was stirred at 50 °C for 48 h to produce a viscous solution. Then, the reaction mixture was cooled to room temperature and poured into hexane (1000 mL). The precipitate was filtered off and dried in vacuo to afford **PU-NP-1%** as a rubbery solid.

II. Theoretical calculation

The initial structure of **D-Ny** and **A-Py-1** was prepared using "gentor+molclus" and Gaussview. The geometrical configuration parameters were optimized using the DFT/BLYP 6-31g method in Gaussian 09w. The electrostatic potential (ESP) distribution on molecular surfaces and intermolecular interactions were ayalyzed and mapped by Multiwfn16.3 combined with VMD1.9.3. to predict binding energies (BEs) based on the electron density at the bond critical point (BCP; ρ_{BCP}) of H-bond. The electron cloud density in the region of the triple H-bond were calculated by Multiwfn16.3. As shown in Fig 2c, the electron density at the bond critical point (BCP; ρBCP) was found as $\rho_{(BCP1)}$=0.06063, $\rho_{(BCP2)}$=0.06022, $\rho_{(BCP3)}$=0.05650). For neutral complexes, the bonding energy was calculated following equation (S1):

$$E_{(\text{H-bond})} = -223.08 \times \cdot \rho_{(BCP)} + 0.7423 \qquad \text{(S1)}$$

III. Experimental calulation on the binding constant of the triple H-bond

Followed by the addition of **A-Py** (10^{-2} mol/L) in THF (4 μL) at a time, the PL spectra of **D-Ny** (10^{-5} mol/L) in THF (1 mL) were recorded until the spectrum maintained stable. The concentration of **A-Py** in solution was changed from 4×10^{-5} mol/L to 1.8×10^{-3} mol/L (the effect of trace amounts of **A-Py** on solution volume was neglected). Taking the reciprocal of the corresponding concentration (***1/[A-Py]***) as the horizontal coordinate, and the difference ($\boldsymbol{I_{max}}$***-I***) between the intensities corresponding to the horizontal coordinate (***I***) and the maximum intensity ($\boldsymbol{I_{max}}$) than the difference (***I-*** $\boldsymbol{I_{min}}$) between the intensities corresponding to the horizontal coordinate (***I***) and the minimum intensity ($\boldsymbol{I_{min}}$) as the vertical coordinate (***(*** $\boldsymbol{I_{max}}$***-I)/(I-*** $\boldsymbol{I_{min}}$***)***), a linear fit was performed to obtain the plot in Fig. 4b with fitting formula as followed：

$$y = 5.90\times10^{-4}x - 0.5711 \ \ (\chi^2 = 0.99825) \qquad \text{(S2)}$$

According to the fitting function, the slope is $k = 5.90 \times 10^{-4}$, $\frac{1}{k} = 1,694.915$. The binding constant $k_a \approx 1.694 \times 10^3 mol/L$ was obtained.

IV. The DSC characterization of the samples

The enthalpy values of melting transition can be determined using the following methodology: the y-axis denotes (heat flow) / weight (unit: W / g), while the x-axis represents Time (unit: s) for the generation of a DSC curve, as illustrated below:

$$\frac{w}{g} = \frac{J/s}{g} = \frac{J}{gs} \qquad \text{(S3)}$$

The integral values of the blue and red areas correspond to the enthalpy changes of the soft segments (unit: J / g), which are -24.90 J/g and -0.001 J/g, respectively.

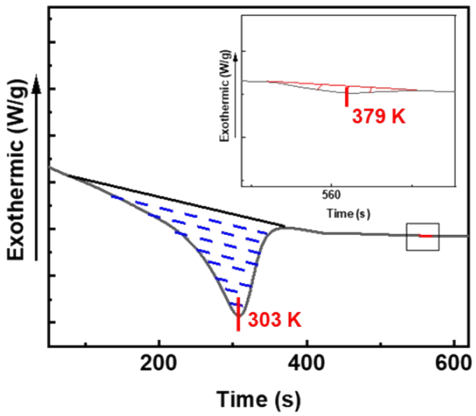

Fig. S1 DSC curve of **PU-NP-1%.**

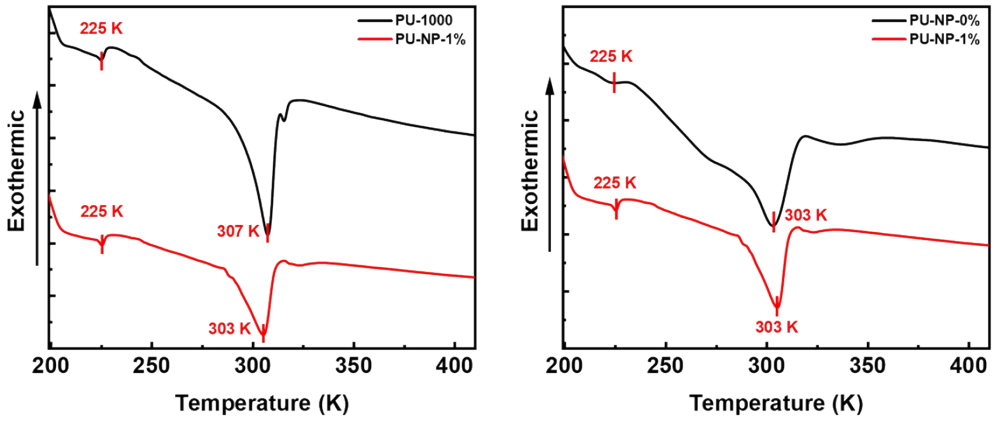

Fig. S2 DSC curves of (a) **PTHF 1000** and **PU-NP-1%**, (b) **PU-NP-0%** and **PU-NP-1%**.

All samples **PU-NP-0.5%**, **PU-NP-1% and PU-NP-2%** showed similar DSC curves with the melting temperature of the soft segments ranging from 297 to 303 K, indicating the amount of the fluorescent probe played minor role in the melting behavior of the soft segment.

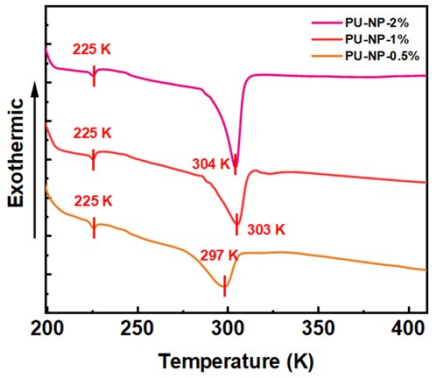

Fig. S3 DSC curves of **PU-NP-0.5%, PU-NP-1%** and **PU-NP-2%**.

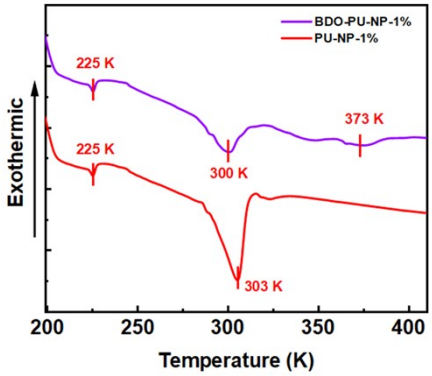

Fig. S4 DSC curves of **PU-NP-1%** and **BDO-PU-NP-1%**.

V. The PL spectra of the PU samples in different temperatures

The temperature-dependent PL spectra indicated that the content of the fluorescent probe significantly influenced the indicative effect after the melting temperature of the soft segment.

In the case of **PU-NP-0.5%**, the initial fluorescence was in quite a high intensity, implying the H-bond complexes were in de-bond dominated state due to the small amount. The intensity was increased with the temperature, and reached the maximum level around the melting temperature of the

soft segment (297 K). Further increasing the temperature led to the decrease of the fluorescent intensity, indicating the increased bonding tendency by means of the increased free volume of the soft segment. However, the PL intensity was re-increased when the temperature was over the melting temperature of the hard segment (373 K), which may reflect the interrupt of the triple H-bond by the interchain interactions in the molten state suffered from the small amount (Fig. S5a, S5d).

For **PU-NP-2%** with a higher probe content, the fluorescent intensity was increased and reached the highest level in the range of the melting temperature of the soft segment (303 K). Upon further heating, the intensity was decreased until a plateau in the melting temperature range of the hard segment (373 K), indicating that thanks to the higher concentration, the bonding and de-bonding tendencies of the triple H-bond realized a dynamic equilibrium even in the molten state of the polymer (Fig. S5c, S5f).

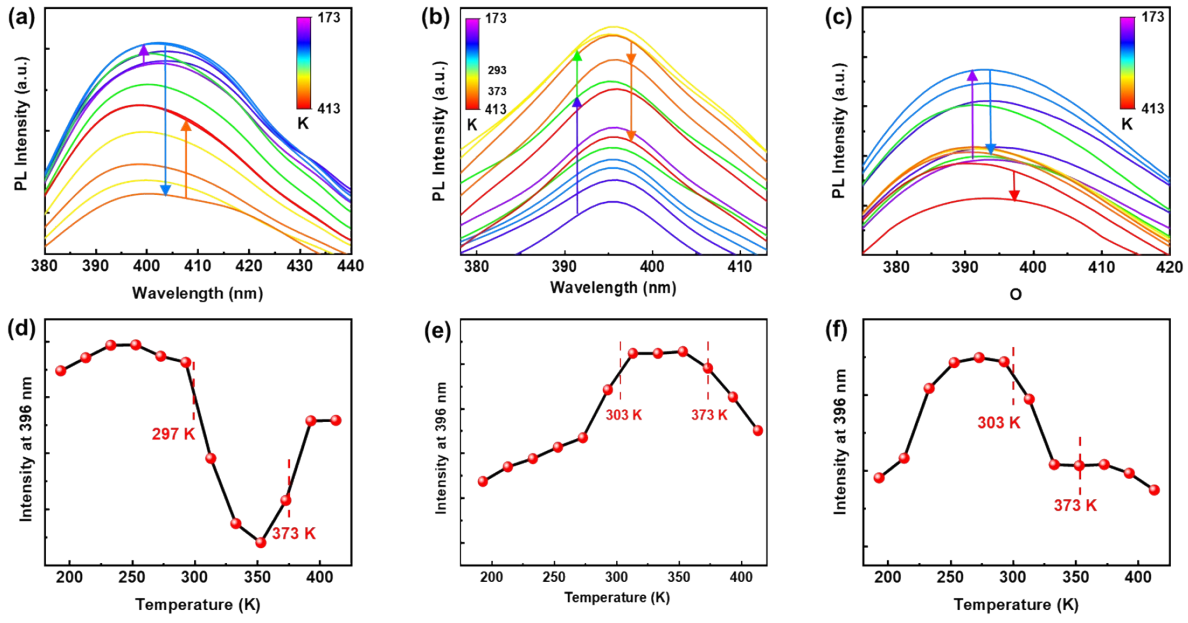

Fig. S5 The PL spectra of (a)**PU-NP-0.5%**, (b) **PU-NP-1%** and (c) **PU-NP-2%** in different temperatures and the PL intensity recorded upon increasing the temperature of (d) **PU-NP-0.5%**, (e) **PU-NP-1%** and (f) **PU-NP-2%**.

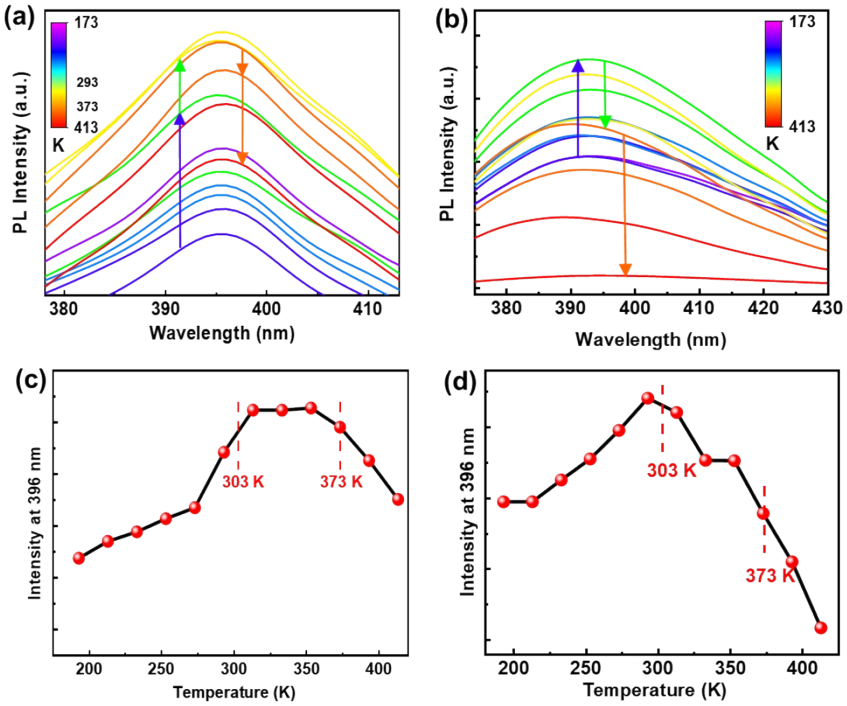

Fig. S6 The PL spectra of (a) **PU-NP-1%**, (b) **BDO-PU-NP-1%** in different temperatures and the PL intensity recorded upon increasing the temperature of (c) **PU-NP-1%**, (d) **BDO-PU-NP-1%**.

VI. GPC curve of polyurethane PU-NP-1%

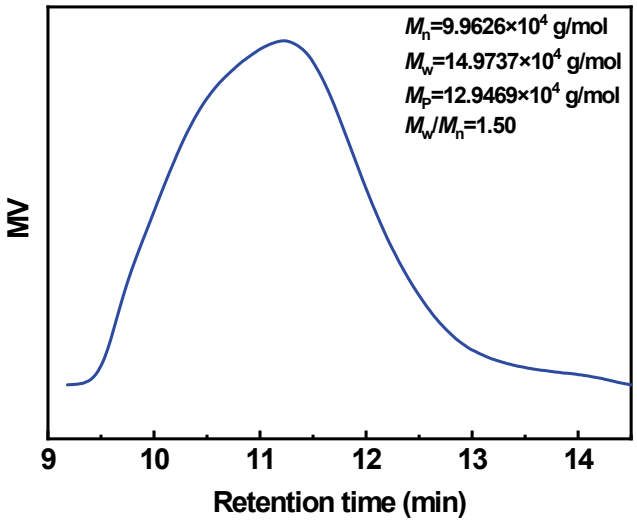

Fig. S7 GPC curve of **PU-NP-1%**.

VII. Stress-strain curves of PU-NP-0%, PU-NP-0.5%, PU-NP-1%, and PU-NP-2%

PU-NP-0.5% containing 0.5% of dynamic chain-extenders showed almost similar mechanical properties to **PU-NP-0%**. When the content was increased to 1% (**PU-NP-1%**), the ductility of PU was effectively maintained while the elastic modulus was significantly enhanced. With 2% content of the dynamic chain-extenders (**PU-NP-1%**), the elastic modulus and ductility were decreased significantly.

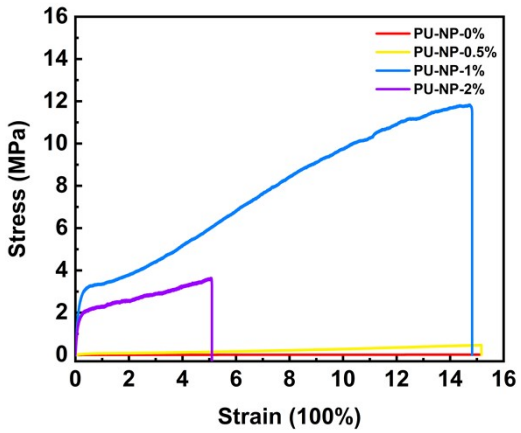

Fig. S8 Stress-strain curve of **PU-NP-0%**, **PU-NP-0.5%**, **PU-NP-1%**, and **PU-NP-2%**.

VIII. ^{1}H and ^{13}C NMR spectra

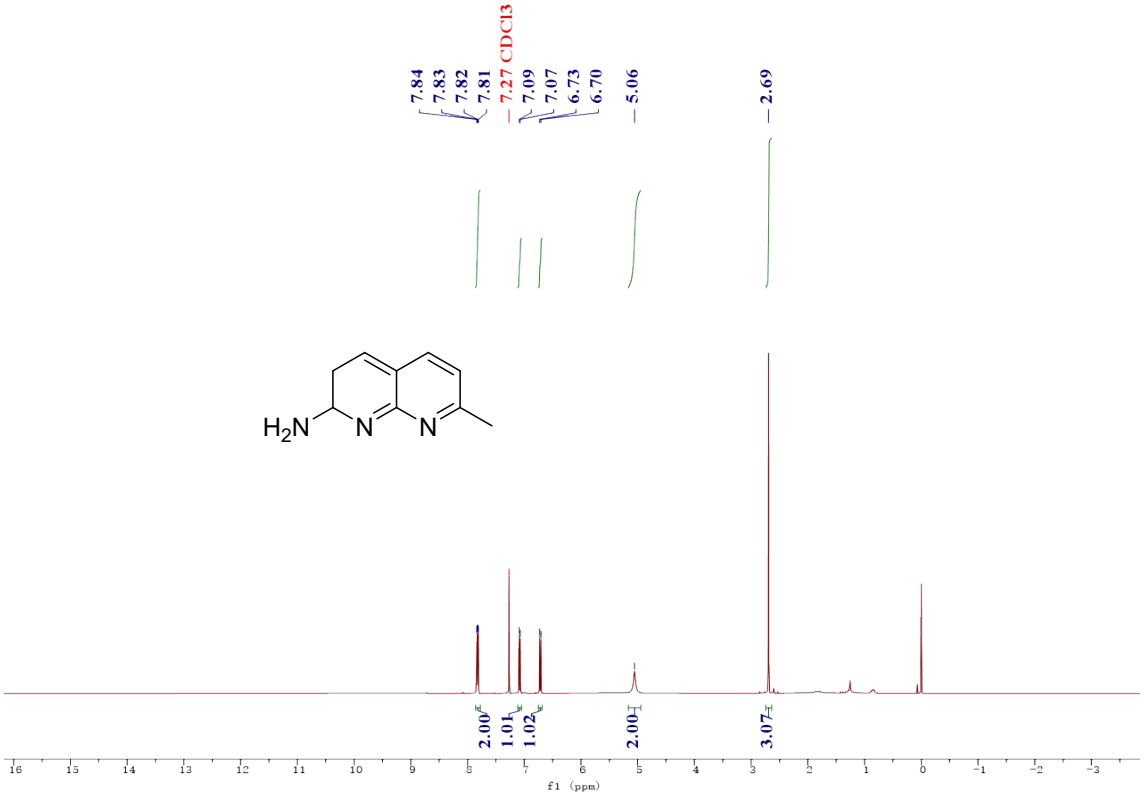

Fig. S9 ^{1}H NMR spectrum of **D-Ny**.

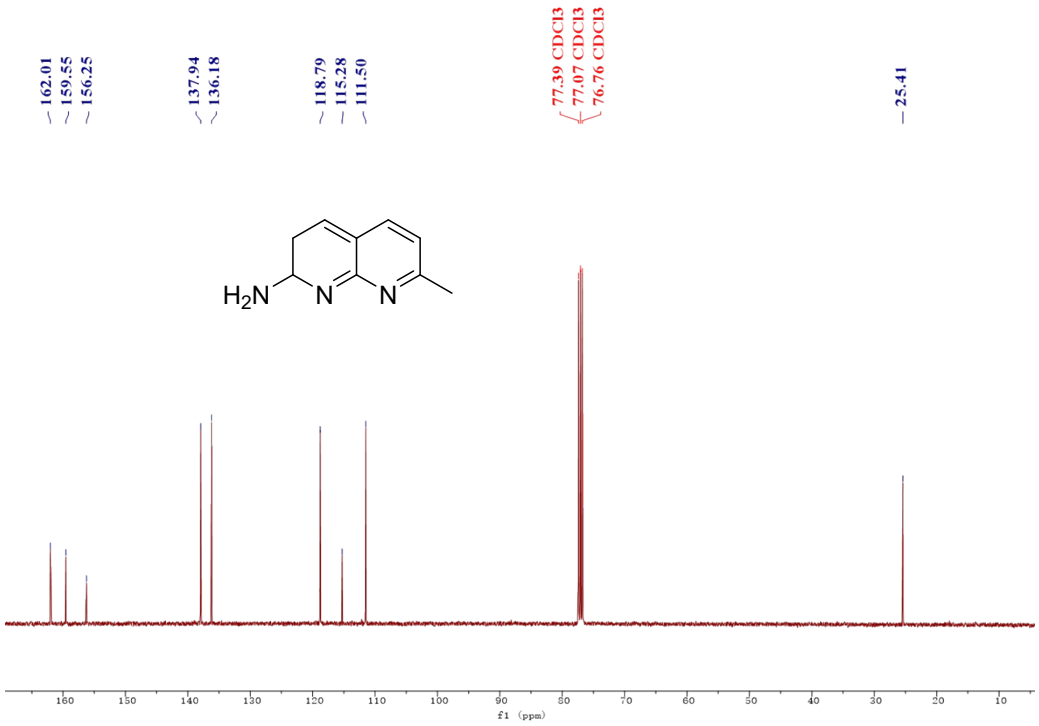

Fig. S10 ^{13}C NMR spectrum of **D-Ny**.

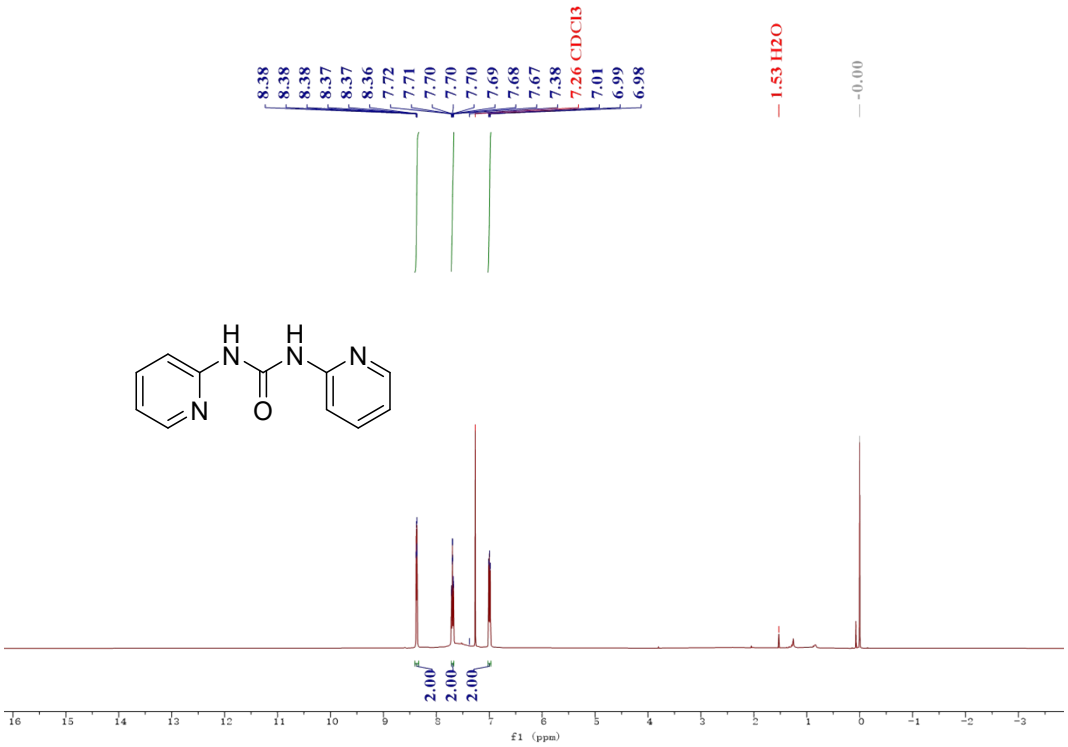

Fig. S11 ^{1}H NMR spectrum of **A-Py**.

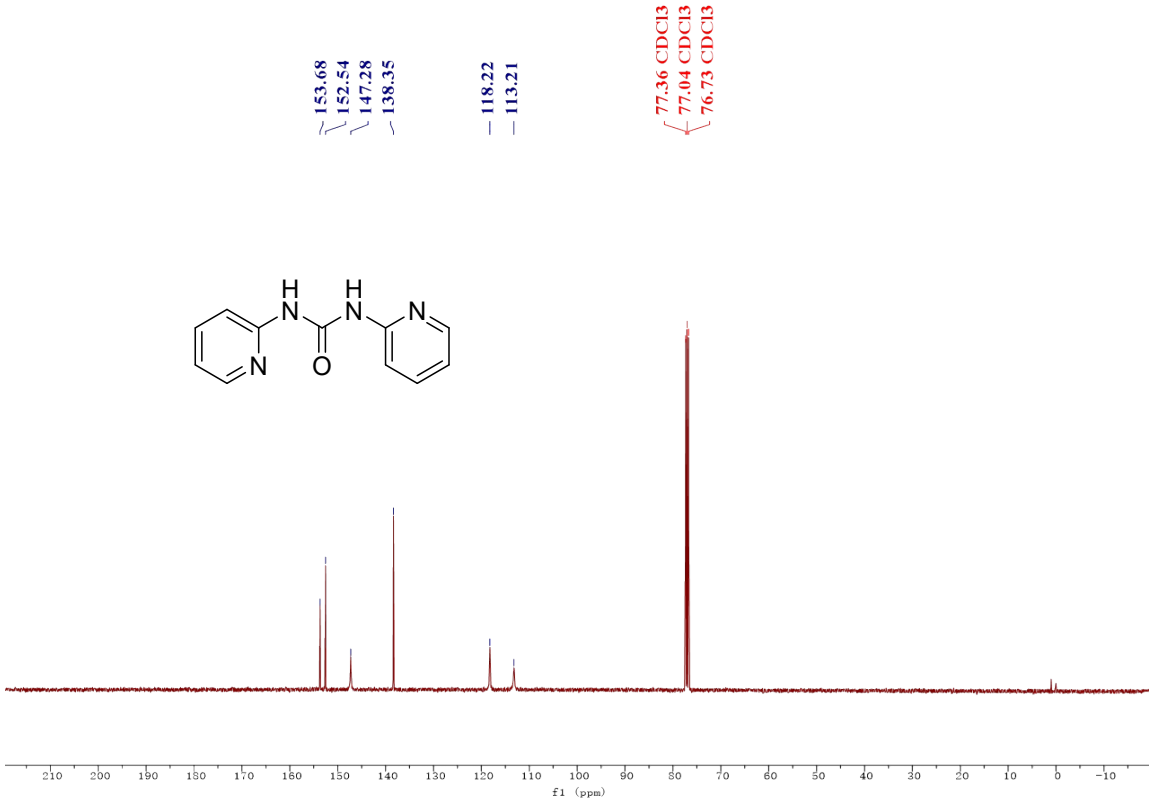

Fig. S12 ^{13}C NMR spectrum of **A-Py**.